IET Power Electronics

Research Article

IET Journals
The Institution of Engineering and Technology

Modelling, control and realisation of the single-ended forward converter with resonant reset at the secondary side

ISSN 1755-4535
Received on 23rd December 2014
Revised on 18th April 2015
Accepted on 1st May 2015
doi: 10.1049/iet-pel.2014.0956
www.ietdl.org

Gierri Waltrich ✉, *Ivo Barbi*

Electrical Engineering Department, Federal University of Santa Catarina, Florianópolis, Brazil
✉ *E-mail: gierri@gmail.com*

Abstract: This study presents modelling, control and realisation of a forward converter with resonant reset at the secondary side. The transformer reset occurs through the resonance between its magnetising inductance and the resonant capacitor during the switch off time. The mechanism is similar to a forward converter with resonant reset at the primary side. The only difference is that the transformer-stored energy can now be partially delivered to the load instead of being dissipated in the switch at turn-on. Another advantage compared with conventional forward converters is the lower switch voltage stress and transformer size, which are theoretically proved to be lower. Furthermore, this converter can be used as a step-up and step-down converter. To verify all the mentioned features, simulations were carried out and a 600 W prototype was implemented experimentally, reaching a maximum efficiency of 94.3%.

1 Introduction

A single-ended forward converter is a well-known topology normally used for low-power applications [1–3]. In this topology, it is necessary to demagnetise the transformer core flux during the switch off period to avoid core saturation. Therefore an auxiliary winding is added to the transformer to reset the flux and to limit the voltage across the converter main switch.

Therefore to avoid the use of this additional winding, a few researches [2, 4] have proposed alternative solutions, which are mainly composed of RCD reset circuits, dual switches and resonant reset circuits.

A topology using RCD circuits is proposed by Gu *et al.* [5] Wei *et al.* [6] and Jovanovic *et al.* [7]. The main advantage of this topology is the wide input voltage range, because the duty cycle can be higher than 50%. However, this topology is composed of an additional switch and an RCD circuit. These additional components increase the converter size and decrease its efficiency.

Another solution to avoid additional winding and reduce voltage stress across the main switches is the use of dual switch [8–12]. The voltage across each switch is the same as the input voltage; however, a complex auxiliary circuit is added.

A simpler and lower cost solution to eliminate auxiliary winding is to use resonant reset topologies [13–18]. In these topologies, a capacitor is added in parallel to the main switch. The transformer reset occurs through the resonance between its magnetising inductance and the resonant capacitor during the switch off time. During the switch on time, the energy is dissipated in the switch increasing the losses in this device.

Therefore to avoid this extra dissipation on the main switch, a capacitor can be placed in parallel to the rectifier diode at the secondary side [18], as shown in Fig. 1. The mechanism of this converter is similar to conventional resonant reset forwards. The main difference is that the transformer-stored energy can now be partially delivered to the load instead of being dissipated in the main switch.

The average voltage across C_R has the same value of the average output voltage and the peak voltage across the switch is controlled by the duty cycle as shown in the following sections. Using this technique, the voltage can be reduced when compared with conventional forward converters. Furthermore, the transformer size can also be reduced, as theoretically proved. Furthermore, the external characteristic of the converter also shows a behaviour similar to a zeta converter, as will be shown later.

To validate all the mentioned characteristics, a 600 W prototype was modelled and implemented experimentally for an input and an output voltage of, respectively, 400 and 60 V. The experimental results show a maximum efficiency of 94.3%.

2 Theoretical analysis

The converter shown in Fig. 1 is similar to a conventional forward converter. The only difference is the capacitor placed in parallel with the rectifier diode (D_R). With this configuration, it is possible to eliminate the demagnetising winding as discussed before. The converter has three different operational stages, as shown in Fig. 2, and detailed in the following subsection. For modelling the converter, the output inductor ripple current (i_L) is considered very low and the transformer is substituted by a single inductor to facilitate the calculations.

2.1 Operational stages

In the first operational stage ($t_0 < t < t_1$), the switch S is turned on and the switch and input currents (i_{DC}) are the same. The voltage over the magnetising inductance is constant in this stage, and therefore, the current on this device grows linearly.

The voltage across L_o can be found by summing the input (V_{DC}), the output (V_o) and the resonant capacitor voltage (v_{CR}), as shown in Fig. 3.

In the first stage the voltage in C_R is positive; thus, the diode D_R is blocked until the voltage in C_R becomes zero, which occurs in the end of the first operational stage (t_1). As the ripple current in i_L is considered very low, that is, almost constant, v_{CR} decreases linearly as shown in Fig. 3.

The proposed converter can operate in two different modes, that is, when the voltage across v_{CR} is working in discontinuous mode ($\gamma T < dT$), or when v_{CR} is working in continuous mode ($\gamma T > dT$). However, in this paper the discontinuous mode ($\gamma T < dT$) is only investigated, because when it operates in continuous mode ($\gamma T > dT$) the converters work exactly as a zeta converter.

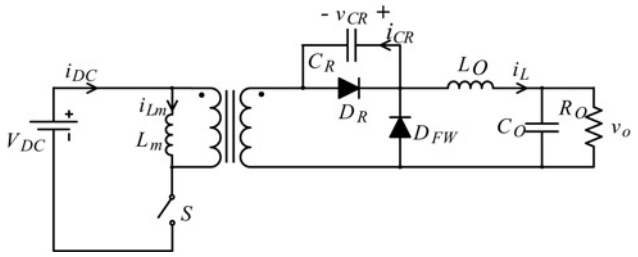

Fig. 1 *Forward converter with resonant reset at the secondary side*

For this converter, the voltage across C_R is considered discontinuous; thus, this capacitor should be completely discharged before the beginning of the next operational stage. The total period of the first stage is defined by C_R and represented by γT.

In the second operational stage ($t_1 < t < t_2$), the switch S is still turned on. This stage begins when C_R is completely discharged. Therefore D_R naturally starts to conduct until the switch S is turned off. The total period of the second operational stage is equal to $(d–\gamma)T$. The voltage across L_o is now equal to $V_{DC}–V_o$. Owing to the low ripple current of i_L, the transformer secondary current has approximately the same value of i_{Ro} in the first two stages.

During the third stage the resonant reset of the transformer occurs. When the switch S is turned off the free-willing diode (D_{FW}) starts to conduct and L_m and C_R are now in series creating a resonant circuit. At this moment (t_2) v_{CR} is null and its voltage value starts to grow in a sinusoidal way. The voltage v_{CR} will increase until a certain value determined by a period $(1–d)T$ where v_{CR} reaches its final value. The currents i_{CR}, i_{L_m} and i_{sec} are equal and have a co-sinusoidal waveform, as shown in Fig. 3. The voltage across L_o is now equal to $–V_o$.

2.2 Resonant components

In this subsection, the resonant components, that is, L_m and C_R are determined. To properly design these components, the operational stages are investigated as follows.

During the first two operational stages the voltage across L_m is equal to V_{DC}, and therefore i_{L_m} rises linearly from a minimum ($i_{L_{m\text{-}min}}$) up to a maximum ($i_{L_{m\text{-}max}}$) value. As shown in Fig. 3, when i_{CR} reaches its maximum value, that is, $i_{CR} = i_{L_{m\text{-}max}}$, the voltage across C_R is null. At this moment (t_2) v_{CR} starts to grow in a sinusoidal way. Thus, it is possible to write

$$v_{CR}(t) = -v_{L_m}(t) = -L_m \frac{d(i_{L_m}(t))}{dt} \tag{1}$$

At this operational stage $i_{CR} = i_{L_m}$; therefore

$$i_{L_m}(t) = i_{CR}(t) = C_R \frac{d(v_{CR}(t))}{dt} \tag{2}$$

Substituting (2) into (1), we obtain

$$\frac{d^2(v_{CR}(t))}{dt^2} + \frac{v_{CR}(t)}{L_m C_R} = 0 \tag{3}$$

By Laplace's transformation, (3) can be solved and its solution is

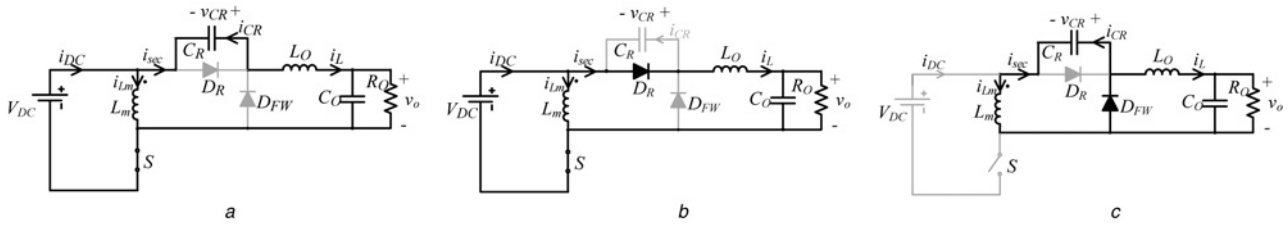

Fig. 2 *Topological stages of the resonant reset forward converter*

a First stage
b Second stage
c Third stage

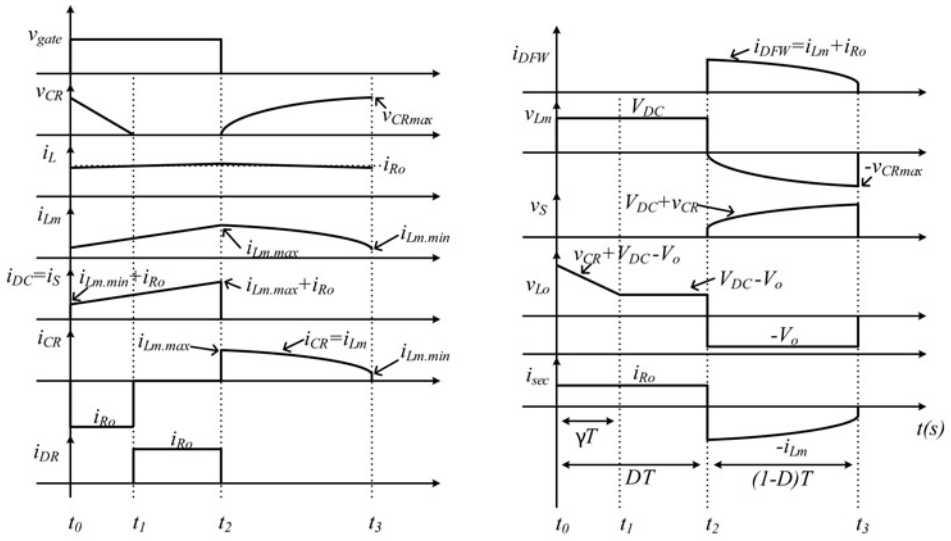

Fig. 3 *Resonant reset forward converter waveforms*

IET Power Electron., 2015, Vol. 8, Iss. 11, pp. 2097–2106

given by

$$v_{CR}(t) = \omega_r L_m i_{L_{m\cdot max}} \sin(\omega_r t) \tag{4}$$

where ω_r is the resonant frequency and is given by

$$\omega_r = 2\pi f_r = \frac{1}{\sqrt{L_m C_R}} \tag{5}$$

Thus, v_{CR} will reach its maximum value when $t = (1-d)T$, and the maximum voltage across C_R is equal to

$$v_{CRmax} = \omega_r L_m i_{L_{m\cdot max}} \sin\left[2\pi \frac{f_r}{f}(1-d)\right] \tag{6}$$

where f is the switching frequency.

To find $i_{L_{m\cdot max}}$ the expression of the current through the resonant capacitor is used. This expression is defined by

$$i_{CR}(t) = C_R \frac{d(v_{CR})}{dt} = i_{L_{m\cdot max}} \cos(\omega_r t) \tag{7}$$

The minimum current through C_R is obtained when $t = (1-d)T$ is substituted into (7), resulting in

$$i_{L_{m\cdot min}} = i_{L_{m\cdot max}} \cos\left[2\pi \frac{f_r}{f}(1-d)\right] \tag{8}$$

The expression for i_{L_m} in the first two operational stages (referenced for the secondary side) is given by

$$i_{L_m}(t) = i_{L_{m\cdot min}} + \frac{V_{DC} n}{L_m} t \tag{9}$$

where n is the transformer turn ratio ($n = Ns/Np$).

The maximum current through $L_m(i_{L_{m\cdot max}})$ occurs when $t = dT$. Thus, considering $t = dT$ and substituting (8) into (9) result in

$$i_{L_{m\cdot max}} = \frac{V_{DC} nd}{f L_m} \frac{1}{1 - \cos\left[2\pi(f_r/f)(1-d)\right]} \tag{10}$$

and substituting (10) into (8), $i_{L_{m\cdot min}}$ is given by

$$i_{L_{m\cdot min}} = \frac{V_{DC} nd}{f L_m} \frac{\cos\left[2\pi(f_r/f)(1-d)\right]}{1 - \cos\left[2\pi(f_r/f)(1-d)\right]} \tag{11}$$

Therefore Δi_{L_m} can be defined as

$$\Delta i_{L_m} = i_{L_{m\cdot max}} - i_{L_{m\cdot min}} = \frac{V_{DC} nd}{f L_m} \tag{12}$$

From (12), it is possible to determine the transformer magnetising inductance by

$$L_m = \frac{V_{DC} nd}{f \Delta i_{L_m}} \tag{13}$$

Usually, Δi_{L_m} is specified as 10–30% of the input current. L_m in (13) is referred to the secondary side.

Once $i_{L_{m\cdot max}}$ is determined by (10), it can be substituted into (6) and the maximum value across the resonant capacitor becomes equal to

$$v_{CRmax} = 2ndV_{DC}\pi \frac{f_r}{f} \frac{1}{\tan\left[\pi(f_r/f)(1-d)\right]} \tag{14}$$

The C_R value is obtained, substituting (13) into (5), resulting in

$$C_R = \frac{1}{L_m (2\pi f_r)^2} \tag{15}$$

As the resonant frequency (f_r) is not a converter specification, it will be calculated considering the following conditions: the output current has very low ripple, the input power is equal to the output power and f_r should have its value much higher, or lower, compared with the switching frequency. The first step to determine f_r is to find the relationship between the output power and C_R and L_o.

The voltage through L_o is shown in Fig. 3 and its average value is null, and is given by

$$v_{L_o} = 0 = \frac{1}{T}\left[\begin{array}{c}\displaystyle\int_{t_0}^{t_1}\left[v_{CR\,max}\left(-\frac{t}{\gamma T}+1\right) + nV_{DC} - V_o\right]dt \\ \displaystyle + \int_{t_1}^{t_2}(nV_{DC} - V_o)dt + \int_{t_2}^{t_3}(-V_o)dt\end{array}\right] \tag{16}$$

Substituting (14) into (16) it is possible to find γ, and is given by

$$\gamma = \frac{f}{\pi f_r}\left(\frac{V_o}{V_{DC} nd} - 1\right)\tan\left[\pi \frac{f_r}{f}(1-d)\right] \tag{17}$$

The current through C_R is shown in Fig. 3 and its average value is also null. Thus, the average value in the negative part of i_{CR} should be equal to its positive part, as described by

$$i_{CR} = 0 = \frac{1}{T}\left[\int_{t_0}^{t_1}(-i_{Ro})dt + \int_{t_2}^{t_3}\left(i_{L_{m\cdot max}}\cos(\omega_r t)\right)dt\right] \tag{18}$$

$$-i_{Ro}\gamma + i_{L_{m\cdot max}} \frac{f}{2\pi f_r} \sin\left(\frac{2\pi f_r}{f}(1-d)\right) = 0 \tag{19}$$

Thus, substituting (10) into (18) and solving the integrals

$$\frac{V_{DC} nd}{L_m 2\pi f_r} \frac{\sin\left(2\pi(f_r/f)(1-d)\right)}{1 - \cos\left[2\pi(f_r/f)(1-d)\right]} = i_{Ro}\gamma \tag{20}$$

By trigonometric identities it is possible to prove that

$$\frac{\sin\left(2\pi(f_r/f)(1-d)\right)}{1 - \cos\left[2\pi(f_r/f)(1-d)\right]} = \frac{1}{\tan\left[\pi(f_r/f)(1-d)\right]} \tag{21}$$

Thus, substituting (17) and (21) into (20), and considering $i_{Ro} = P_o/V_o$, f_r can be given by

$$f_r = \frac{f}{\pi} \cdot \frac{1}{1-d} \cdot \arctan\left[\frac{V_{DC} nd}{\sqrt{2P_o L_m f(1 - (V_{DC}/V_o)nd)}}\right] \tag{22}$$

where P_o and V_o are, respectively, the output power and voltage. Finally, substituting (22) into (15) it is possible to determine the C_R value.

2.3 Converter output characteristic

To compare the proposed converter with the conventional forward topology, its output characteristic should be found. It is well-known that the forward output characteristic is given by

$$\frac{V_o}{nV_{in}} = d \tag{23}$$

Therefore, its output voltage is always lower or equal to the input voltage, if, for instance, $n = 1$. The same can be made for the

proposed converter. To find the V_o/V_{in}, that is, the output characteristic, (22) is used, but in this case the input voltage is equal to V_{DC}. Thus, isolating V_o/nV_{DC} from (22) and considering $i_L \simeq i_{Ro} = P_o/V_o$, that is, very low output current ripple, the output characteristic of the proposed converter is given by

$$\frac{V_o}{nV_{DC}} = d + \frac{d^2}{\overline{i_L}} \cdot \frac{1}{\left[\tan\left[\pi(f_r/f)(1-d)\right]\right]^2} \tag{24}$$

where $\overline{i_L}$ is the output current normalised by

$$\overline{i_L} = \frac{2L_m f}{V_{DC} n} i_L \tag{25}$$

The converter output characteristic given by (24) is shown in Fig. 4. From this figure it is demonstrated that the resonant reset forward has the output characteristic similar to a buck–boost converter ($d/1-d$), that is, the proposed converter can be used as a step-up or step-down converter. The reason why these two converters present similar characteristics is due to the similar mechanism of store energy between operational stages. The difference is that the buck–boost converter stores energy in an inductor in one operational stage and releases it in the next stage, whereas the resonant reset forward converter do the same mechanism but using the additional capacitor (C_R) placed in the secondary side. Thus, the resonant reset forward converter can be used as a step-up and a step-down converter.

2.4 Transformer design

To design the transformer, root mean square (RMS) current and voltage in the primary and secondary sides should be determined. The RMS current in the primary and the secondary side is given, respectively, by

$$i_{pri} = \frac{n\sqrt{d}}{2L_m f} \cdot \frac{1}{(1/V_{DC}nd) - (1/V_o)} \cdot \frac{1}{\left[\tan\left[\pi(f_r/f)(1-d)\right]\right]^2} \tag{26}$$

$$i_{sec} = \frac{ndV_{DC}}{L_m f} \cdot \sqrt{\frac{d(ndV_{DC})^2}{4(V_o - ndV_{DC})^2} \cdot \left(\tan\frac{\alpha}{2}\right)^{-4} + \frac{1-d+(f/4\pi f_r)\sin(2\alpha)}{2(1-\cos\alpha)^2}} \tag{27}$$

and the RMS voltage in the primary and the secondary side is given, respectively, by

$$v_{pri} = V_{DC} \cdot \sqrt{d + \frac{(2\pi f_r d)^2}{f} \cdot \frac{(1-d/2) - (f/8\pi f_r)\sin(2\alpha)}{(1-\cos\alpha)^2}} \tag{28}$$

$$v_{sec} = v_{pri} n \tag{29}$$

Therefore to calculate the apparent power in the output and the input of the transformer simply multiply the RMS voltage and current on each side.

2.5 Semiconductor design

In this subsection, the semiconductor components of the resonant reset forward components are designed. All the parameters are calculated using the waveforms shown in Fig. 3 as a reference.

To properly design the switch, it is necessary to determine the RMS and the peak value for both current and voltage. The peak voltage value across the main switch is equal to V_{DC} plus the maximum voltage across C_R. Substituting (11) into (6), and adding the resulting equation with V_{DC}, the maximum voltage across the main switch is given by

$$v_{S\,peak} = V_{DC}\left[1 + 2\pi nd\frac{f_r}{f}\frac{1}{\tan\left[\pi(f_r/f)(1-d)\right]}\right] \tag{30}$$

Equation (30) shows the switch peak voltage duty cycle dependence. Therefore if the resonant components and the duty cycle range are properly designed, it can even have a lower value across the main switch when compared with the conventional forward converter, where the voltage across the main switch is usually equal to $2V_{DC}$. For instance, using the parameters from Table 1, the switch peak voltage is equal to 648 V (for $d = 0.25$), which is ~19% lower when compared with the conventional forward converter. Obviously, if a lower duty cycle is used, the peak voltage is also lower. On the other hand, it will increase the current through the components and it will have an impact mainly on the transformer size. Thus, the best way to design this converter is finding a balance between the maximum switch voltage and transformer size.

The current through the converter main switch is equal to the current in the transformer primary side ($i_{primary}$), and the peak current value on this semiconductor is equal to

$$i_{S\,peak} = i_{L_{m\cdot max}} + i_{Ro} \tag{31}$$

The RMS current expressions for the diodes D_R and D_{FW} were

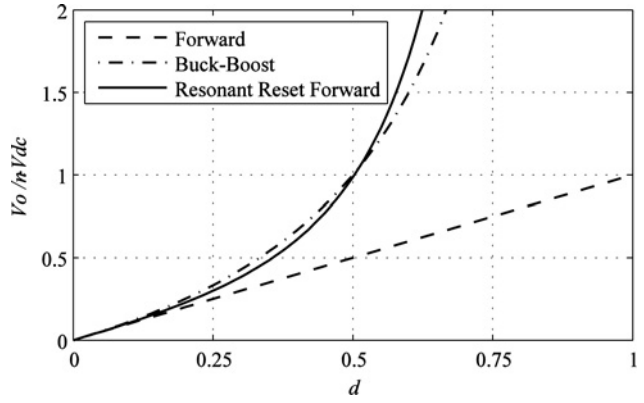

Fig. 4 *Converter output characteristics*

Table 1 Parameters used in numerical simulations and experimentations

Parameter	Value
power	600 W
switching frequency	50 kHz
input voltage	400 V
output voltage	60 V
duty cycle	0.25
transformer turn ratio	1/2
magnetising inductance (L_m)	1.11 mH
resonant capacitor (C_R)	258.0 nF
load resistance (R_o)	6.0 Ω
filter inductance (L_o)	1 mH
filter capacitance (C_o)	100 μF

determined and they are given, respectively, by

$$i_{D_R} = \frac{(ndV_{DC})^2}{2L_m f(V_o - ndV_{DC})} \cdot \frac{\sqrt{d - (f/\pi f_r)((V_o/ndV_{DC}) - 1)\tan(\alpha/2)}}{(\tan(\alpha/2))^2} \tag{32}$$

$$i_{D_{FW}} = \sqrt{i_{Ro}^2 - \frac{1}{2}\left(\frac{ndV_{DC}}{L_m f}\right)^2 \cdot \frac{(1 - d + (f/4\pi f_r)\sin(2\alpha))}{(1 - \cos\alpha)^2}} \tag{33}$$

The RMS current through the resonant capacitor (C_R) was also calculated and its equation is given by

$$i_{C_R} = \frac{ndV_{DC}}{L_m f} \cdot \sqrt{\frac{f/4\pi f_r}{((V_o/dV_{DC}) - 1)} \cdot \left(\tan\frac{\alpha}{2}\right)^{-3} + \frac{1 - d + (f/4\pi f_r)\sin(2\alpha)}{2(1 - \cos\alpha)^2}} \tag{34}$$

2.6 Small-signal modelling

For modelling the resonant reset forward converter, small-signal modelling techniques were used. Small-signal modelling is used to approximate the behaviour of non-linear devices with linear equations. This linearisation is formed about the DC bias point of the device, and can be accurate for small excursions about this point. Therefore the non-linear devices, that is, diodes and switches, on the circuit shown in Fig. 1, were linearised using this technique. However, before starting the linearisation, a simplification of the circuit shown in Fig. 1 will be carried out. When the output characteristic described by (24) was developed, the average voltage across the output filter inductor was considered zero. Therefore V_o in (24) is actually the voltage across the diode D_{FW} ($v_{D_{FW}}$). Thus, $v_{D_{FW}}$ can be substituted by a voltage-controlled voltage source, as shown in Fig. 5*a*, where $v_{D_{FW}}$ is non-linear and is given by

$$v_{D_{FW}} = nV_{DC}d + \frac{nV_{DC}d^2}{\overline{i_L}} \cdot \frac{1}{\left[\tan\left[\pi(f_r/f)(1 - d)\right]\right]^2} \tag{35}$$

and the output voltage, considering the output filter, is given by

$$v_o(s) = v_{D_{FW}}(s)\frac{1}{s^2 L_o C_o + s(L_o/R_o) + 1} \tag{36}$$

The tangent term in (35) for small values around the operation DC bias point is almost linear and can be substituted by a linear expression given by

$$\tan\left[\pi\frac{f_r}{f}(1 - d)\right] \simeq 0.653 - 0.714d \tag{37}$$

where f and d are given in Table 1, and f_r is obtained from (22). Thus, substituting (37) into (35) results in

$$v_{D_{FW}} = nV_{DC}d + \frac{nV_{DC}d^2}{\overline{i_L}} \cdot \frac{1}{(0.653 - 0.714d)^2} \tag{38}$$

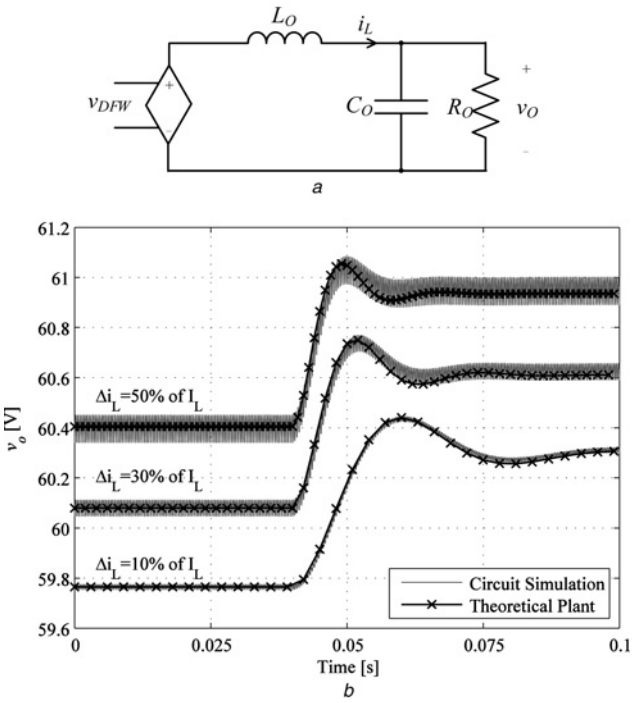

Fig. 5 *Simulation with three different current ripples*

a Circuit used for small-signal modelling
b Comparison between the resulted modelling given by (43) and the simulation on PSIM software for a small disturbance on the duty cycle

For modelling the circuit shown in Fig. 5*a*, the voltage-controlled voltage source ($v_{D_{FW}}$) must be linearised; otherwise, the Laplace transformation cannot be used. To linearise (38), the duty cycle (d), the voltage across the diode D_{FW} ($v_{D_{FW}}$) and the current through L_o($\overline{i_L}$), shown in Fig. 1, should be substituted by their mean value added to a small disturbance, as given by

$$\begin{aligned} v_{D_{FW}} &= \hat{v}_{D_{FW}} + V_{D_{FW}} \\ \overline{i_L} &= \hat{i}_L + \overline{I_L} \\ d &= \hat{d} + D \end{aligned} \tag{39}$$

where $V_{D_{FW}}$, $\overline{I_L}$ and D are the average values at the operational point and $\hat{d}$, $\hat{i}_L$ and $\hat{v}_{D_{FW}}$ are the small perturbations added to their, respectively, average values.

When (39) is substituted into (38) the resultant expression is formed by two different terms – an average and a time-variant term. Regrouping the average term from the resultant expression results in

$$V_{D_{FW}} = \frac{((nV_{DC}D)^2/\overline{I_L} f L_m) - V_{DC}\left(1.864nD^2 - 0.852nD - 1.02nD^3\right)}{0.852 - 1.864D + 1.02D^2} \tag{40}$$

In the same way, regrouping the time-variant terms, disregarding terms with order superior to one, the expression results in (see (41))

$$\begin{aligned} \hat{v}_{D_{FW}} = {} & \frac{V_{DC}(0.852nD - 1.864nD^2 + 1.02nD^3) + V_{D_{FW}}(-0.852 + 1.864D - 1.02D^2)}{\overline{I_L}(0.852 - 1.864D + 1.02D^2)}\hat{i}_L \\ & + \frac{V_{D_{FW}}(-2.04D + 1.864) + V_{DC}(0.852n - 3.728Dn + 3.06nD^2) + (n^2 V_{DC}^2/f L_m \overline{I_L})2D}{0.852_L - 1.864D + 1.02D^2} \end{aligned} \tag{41}$$

Substituting (41) into (36) and the inductor current by

$$\hat{i}_{\mathrm{L}}(s) = sC_{\mathrm{o}}\hat{v}_{\mathrm{o}} + \frac{\hat{v}_{\mathrm{o}}}{R_{\mathrm{o}}} \tag{42}$$

after some mathematical manipulations, the output voltage in function of the duty cycle, that is, the transfer function of the converter, can be written as

$$\frac{\hat{v}_{\mathrm{o}}(s)}{\hat{d}(s)} = \frac{\varepsilon}{s^2(\alpha L_{\mathrm{o}}C_{\mathrm{o}}) + s(\alpha(L_{\mathrm{o}}/R_{\mathrm{o}}) + \beta C_{\mathrm{o}}) + (\alpha + (\beta/R_{\mathrm{o}}))} \tag{43}$$

where

$$\begin{aligned}
\alpha &= \overline{I_{\mathrm{L}}}(0.852 - 1.864D + 1.02D^2) \\
\beta &= V_{\mathrm{DC}}(-0.852nD + 1.864nD^2 - 1.02nD^3) \\
&\quad + V_{D_{\mathrm{FW}}}(0.852 - 1.864D + 1.02D^2) \\
\varepsilon &= \frac{n^2V_{\mathrm{DC}}^2}{fL_{\mathrm{m}}}2D + \overline{I_{\mathrm{L}}}\left[\begin{array}{l} V_{D_{\mathrm{FW}}}(1.864 - 2.04D) \\ \quad + V_{\mathrm{DC}}(0.852n - 3.728Dn + 3.06nD^2) \end{array}\right]
\end{aligned} \tag{44}$$

To validate the transfer function (or converter plant) given by (43), a simulation was carried out using PSIM software. The circuit shown in Fig. 1 was built using ideal components and the parameters shown in Table 1. PSIM software allows to implement the transfer function equation in a block, and therefore, a comparison can be made between the converter circuit and (43). To carry out this comparison, a small disturbance on the duty cycle was given and the output voltage of both models compared, and the result is shown in Fig. 5*b*. This figure shows the similarities between both models, validating (43). In Fig. 5*b* a simulation with three different current ripples, that is, 10, 30 and 50% ripple values calculated over $\overline{i_{\mathrm{L}}}$ is shown. As (43) describes the behaviour of the output voltage (v_{o}), the model will present an error when perturbation on v_{o}, during the commutation period, occurs. As shown in the figure above, with larger current ripples the perturbations on v_{o} increases, and consequently, the difference between model and simulation also increases Despite the three output voltages in the figure above presenting similar average values of v_{o} lower ($\Delta V \leq 0.3$ V), some differences still exist. Since changes on L_{o} should only modify the current ripple, and not the average value of v_{o}, this variation can be explained by Fig. 2*c*. As i_{L} pass through D_{FW} it will change the resonant circuit current shown by Fig. 2*c*, changing the model. Since the changes of the average value of v_{o} are small ($\Delta V \leq 0.3$ V or $\leq$0.5%), it can be discarded. However, changes on the output current ripple are important and they should be considered. Usually, a higher output current ripple is desired to minimise the inductor value (L_{o}), and consequently its size. Thus, if the converter is designed with a higher current ripple a larger output capacitor should be implemented to minimise the perturbation of v_{o}, keeping the model presented by (43) valid.

In Fig. 6*b*, the theoretical frequency responses (amplitude and phase) of the converter plant, defined by (43), is shown. This figure was plotted considering the parameters from Table 1. As shown in Fig. 6*b* and described in (43), the converter plant is a second-order system, like conventional forward converters. Therefore the resonant reset forward converter studied in this paper can be controlled using the same methods and controllers implemented in conventional forward converters [15], as shown in the following subsection.

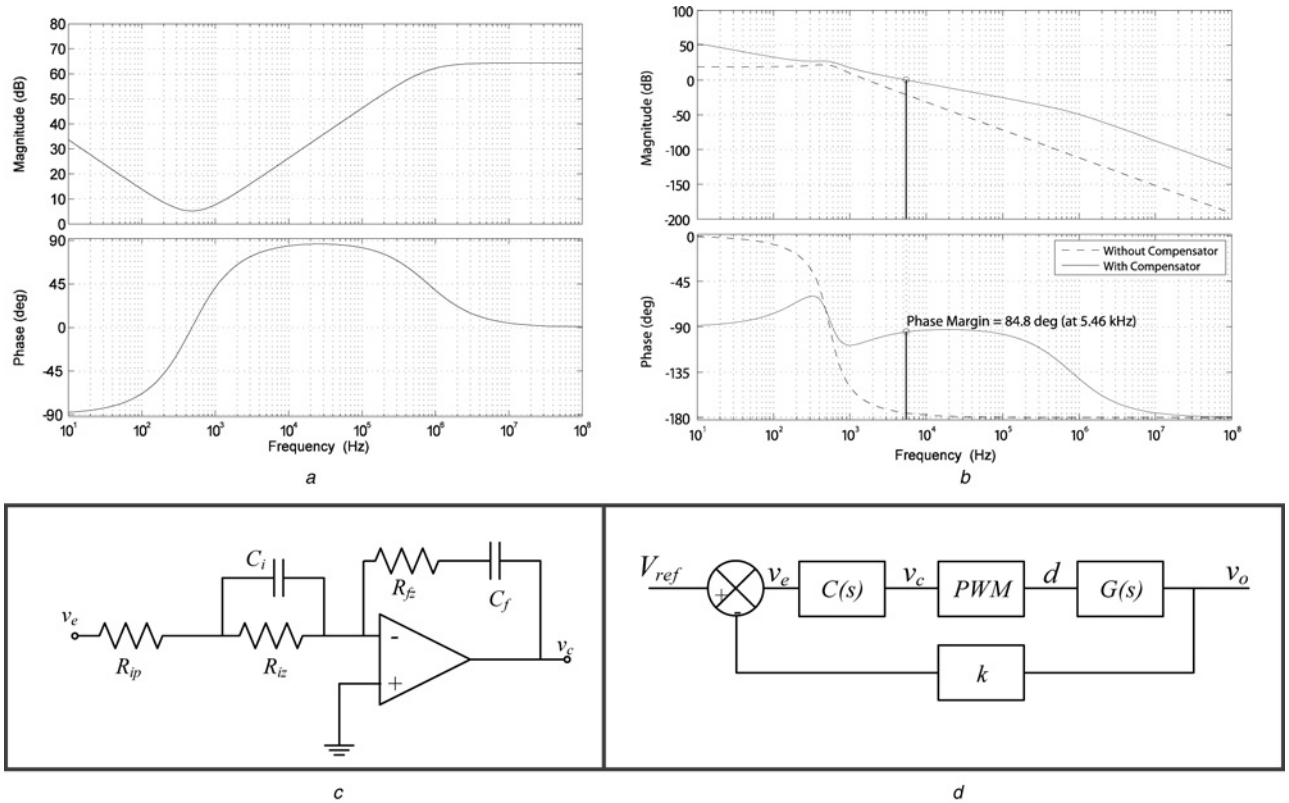

Fig. 6 *Theoretical frequency responses (amplitude and phase) of the converter plant*

a Frequency responses of the two zero two pole compensator
b Converter transfer function with and without compensator
c Lead-phase compensator implemented
d Closed-loop control system

IET Power Electron., 2015, Vol. 8, Iss. 11, pp. 2097–2106

2.7 Control design

The phase margin of the resonant reset forward converter is close to zero, as shown Fig. 6*b*. Therefore the circuit requires a compensator to guarantee circuit stability. The proposed converter has a second-order plant, as described in Fig. 6*b*. To increase the converter phase margin, a few compensators can be used, for instance, using an integral controller, a proportional–integral (PI) controller, among others. If an integral controller is implemented it will increase 90° on the converter plant phase margin, and, therefore, the zero dB crossing frequency (ω_o) should be regulated (changing the gain of the compensator), until the desired phase margin is obtained. On the other hand, if a PI controller is used the phase margin and the compensator gain can be precisely calculated. For both methods, ω_o should be designed for a frequency lower than the converter resonant frequency, and, therefore, the circuit will have a lower dynamic performance. Thus, to increase the converter dynamic performance, a phase-lead compensator can be implemented. One example of a phase-lead compensator is shown in Fig. 6*c*. This compensator provides a positive phase angle close to the zero dB crossing, allowing an improvement in the phase margin. Its transfer function is given by

$$\frac{v_c(s)}{v_e(s)} = \frac{(1 + R_{iz}C_i s)(1 + R_{fz}C_f s)}{sC_f(R_{ip} + R_{iz})(1 + sC_i(R_{ip}R_{iz}/R_{ip} + R_{iz}))} \tag{45}$$

The transfer function given by (45) has two poles and two zeros in the following frequencies

$$\omega_{p1} = 0, \quad \omega_{p2} = \frac{R_{ip} + R_{iz}}{C_i R_{ip} R_{iz}}, \quad \omega_{z1} = \frac{1}{C_i R_{iz}}, \quad \omega_{z2} = \frac{1}{C_f R_{fz}} \tag{46}$$

where, normally, $\omega_{z1} = \omega_{z2} = \omega_o$ and $\omega_{p2} = 5\omega_o$. For this compensator, the two zeros of the transfer function are designed with a frequency higher than the resonant frequency of the converter, increasing the dynamic performance of the system. One of the poles is placed at the origin and the other pole is placed in a frequency five times higher than ω_o. Thus, following the previous constraints the components were determined and their values are

$$R_{ip} = 20\ \Omega, \quad R_{iz} = 33\ \text{k}\Omega, R_{fz} = 33\ \text{k}\Omega, \quad C_i = 10\ \text{nF}, \quad C_f = 10\ \text{nF} \tag{47}$$

The Bode diagram of this compensator is shown in Fig. 6*a*. The positive phase angle near the zero dB crossing improves the phase margin. The DC gain is theoretically infinite, leading to a null steady-state error. Note that the gain is not reduced when the frequency is increased, but the reduction is ensured in closed loop by the output filter, as shown in Fig. 6*b*. Using this compensator, the phase margin increased ensuring circuit stability.

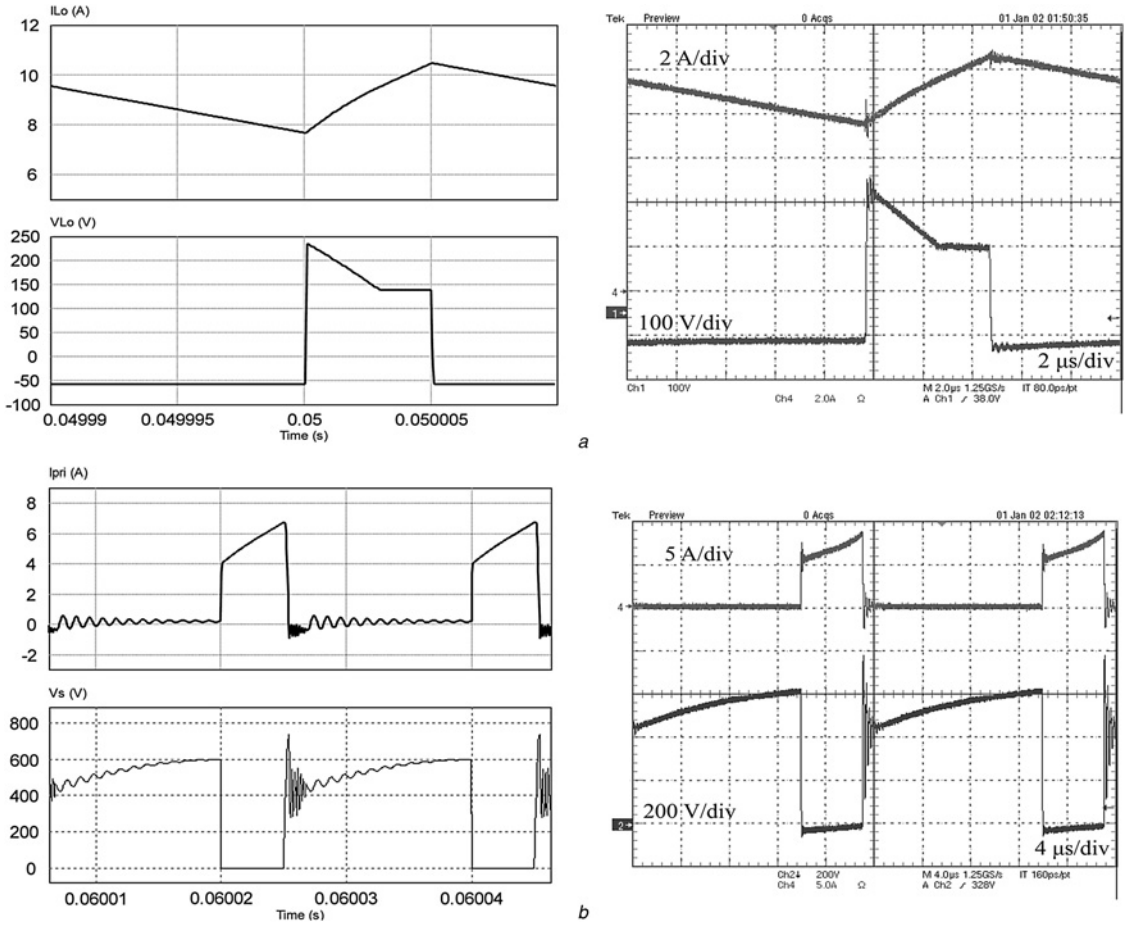

Fig. 7 *Simulation and experimental results for the resonant reset forward converter*

a Current (i_{L_o}) and voltage (v_{L_o}) across L_o
b Input current (i_{pri}) and voltage across the main switch (V_S)

In Fig. 6*d*, the closed-loop system is also shown. The parameters shown in this figure are given by

$$C(s)=\frac{v_c(s)}{v_e(s)},\quad \text{PWM}=\frac{1}{V_{\text{P}}},\quad G(s)=\frac{\hat{v}_{\text{o}}(s)}{\hat{d}(s)}\quad \text{and}\quad k=\frac{V_{\text{ref}}}{V_{\text{o}}} \tag{48}$$

where V_{P} is the peak value of the saw-tooth carrier. Using the parameters given in (48) the transfer function of the complete system can be determined and is given by

$$\frac{\hat{v}_{\text{o}}}{V_{\text{ref}}}=\frac{(\varepsilon/V_{\text{P}})(1+R_{iz}C_i s)(1+R_{fz}C_f s)}{\left[s^2(\alpha L_{\text{o}}C_{\text{o}})+s\left(\alpha(L_{\text{o}}/R_{\text{o}})+\beta C_{\text{o}}\right)+\left(\alpha+(\beta/R_{\text{o}})\right)\right]\\ sC_f\left(R_{ip}+R_{iz}\right)\left(1+sC_i(R_{ip}R_{iz}/R_{ip}+R_{iz})\right)\\ +(\varepsilon/V_{\text{P}})(1+R_{iz}C_i s)(1+R_{fz}C_f s)k} \tag{49}$$

3 Simulation and experimental results

Numerical simulations were performed and a laboratory prototype of 600 W was designed, built and tested to investigate the technical feasibility and to validate the theoretical concepts of the resonant reset forward converter. The specifications used in numerical simulations and experimentations are shown in Table 1 and the results are shown in Figs. 7 and 8.

In Fig. 7*a* the current and voltage across the output filter inductor (L_{o}) is shown. The output ripple current was designed to be at a maximum of 30% of the nominal output current (10 A) to avoid a large filter inductor. As shown in Fig. 7*a*, the current has an output ripple current lower than 3 A and the voltage across $V_{L_{\text{o}}}$ has a waveform similar to the one presented in the theoretical studies shown in Fig. 3.

The input current (or transformer primary current) and the voltage across the main switch are presented in Fig. 7*b*. The average value of the input current was measured, and it was close to 1.5 A, as predicted.

The voltage across the main switches has the maximum value a little bit higher, compared with the theoretical result. It is due to higher transformer leakage inductance referred to the primary side, which is ~4.50 µH. However, if the transformer was more appropriately designed this peak value might decrease. A snubber can also be designed to decrease this peak voltage or soft switching techniques can also be implemented to reduce the losses and increase the converter efficiency as described in [17–20].

With the parameters presented in Table 1 and (26)–(29), the kVa rating of the transformer can be determined. As the voltage and current waveforms in the resonant reset forward transformer are different from the conventional forward, it is expected to give some differences in the kVa rating in both topologies. One way to calculate the kVa rating is to determine both RMS voltage and current of the transformer in both sides and use these RMS values to calculate the apparent power and divide by the active power. Thus, it is possible to determine how big should be the transformer compared with the nominal active power. The relation between the apparent and active power, in the primary and secondary sides are, respectively, 1.20 and 1.07, whereas for the conventional forward converter it is equal to 1.41 on both sides. Therefore the resonant reset forward converter has a reduction of

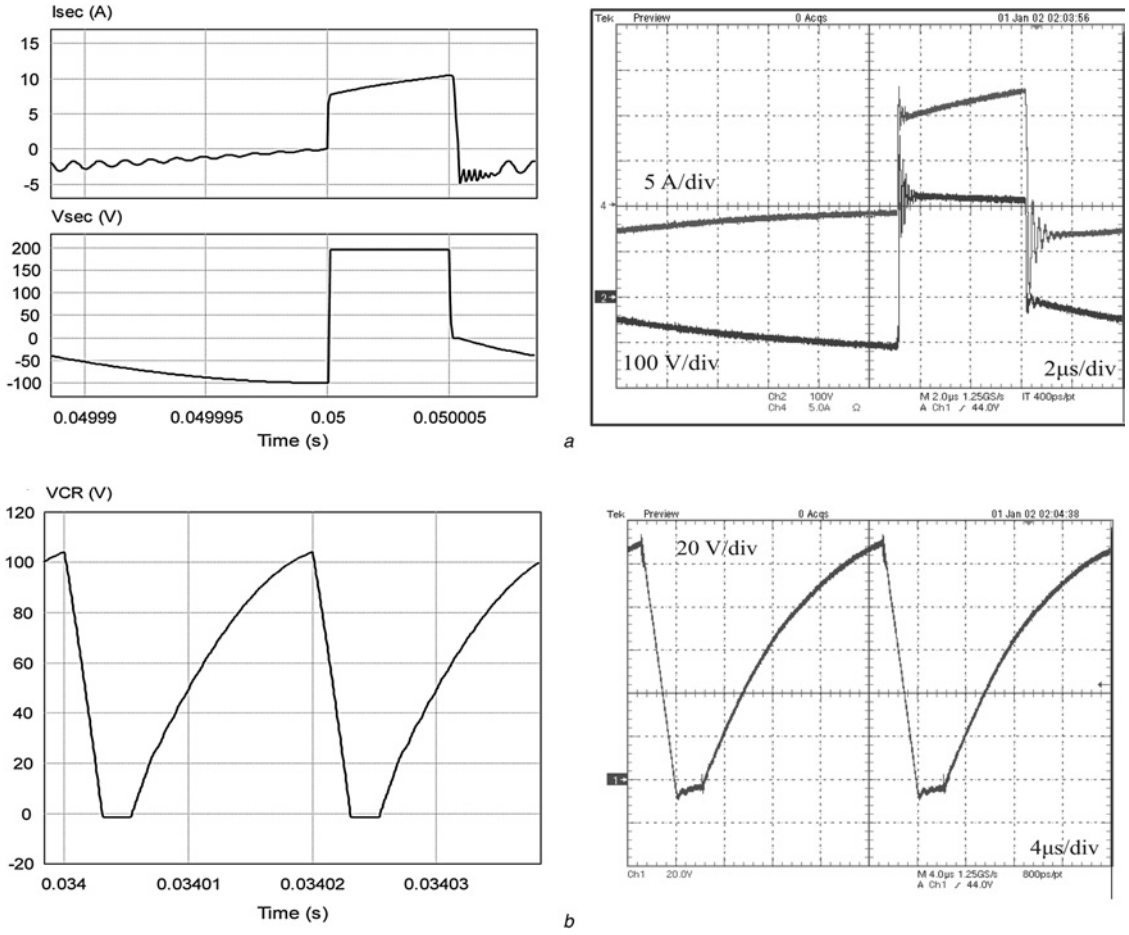

Fig. 8 *Simulation and experimental results for the resonant reset forward converter*

a Current (i_{sec}) and voltage (v_{sec}) on the transformer secondary side
b Voltage across C_{R}

IET Power Electron., 2015, Vol. 8, Iss. 11, pp. 2097–2106

the transformer size by almost 20%, compared with the conventional forward converter.

In Fig. 8*b*, the voltage across C_R is presented. In this graph it is clear that the voltage in this component is operating in discontinuous mode. However, the average voltage value in this component is equal to the output voltage. Fig. 8*b* shows clearly the three operational stages presented in Fig. 2 namely zero voltage, resonant and linear stage.

The converter was also tested in close loop for a changing of 50% in the converter load, that is, from 300 to 600 W, as shown in Fig. 9*a*. The controller was designed to keep the output voltage stable and equal to 60 V. As shown in this figure, after changing 50% of the load, V_o decreases a little bit but it rapidly returns to the nominal value, validating the compensator designed in subsection *G*. The compensator was designed placing both zeros in 482 Hz, one pole at the origin and another pole in 796.25 kHz.

To evaluate the converter efficiency, the experimental prototype was tested for different loads as shown in Fig. 9*b*. The proposed converter presents better efficiency when compared with conventional forward topologies, as shown in [1, 18]. In [1] an efficiency curve for a series-input RCD forward converter with a load power varying from 30 to 210 W, reaching a maximum efficiency of 89% for a 100 W prototype is shown. The proposed converter efficiency was measured in a power range between 70 and 650 W, and reached a maximum efficiency of 94.3% (around 300 W), as shown in Fig. 9*b*. In [1], the authors propose a series-input interleaved RCD forward converter with better efficiency (93–94%); however, it was obtained using four switches and two transformers. Some authors [14, 21] also tried to use the reset capacitor at the transformer primary side, to avoid the use of a demagnetising winding. However, using this method the energy storage in the capacitor is dissipated on the switch, decreasing the converter efficiency. Thus, if this method is implemented soft switching techniques are required or more switches might be used to increase the converter efficiency [2].

Thus, compared with conventional forward topologies, the proposed converter presents some advantages. For instance, it does not have auxiliary winding to demagnetise the transformer; it has lower transformer size, lower peak voltage across the main switch and better efficiency.

The proposed converter reaches this better performance because of the methodology implemented in this paper and because the prototype was built using a silicon carbide power metal–oxide–semiconductor field-effect transistor (MOSFET) (C2M0080120D, CREE, 1200 V), reducing the cooling requirements and increasing the system efficiency.

Using the methodology described in this paper, it is also possible to find a balance between the transformer turn ratio and duty cycle which provides the lowest transformer size, and consequently a lower leakage inductance decrease the peak voltage across the main converter switch.

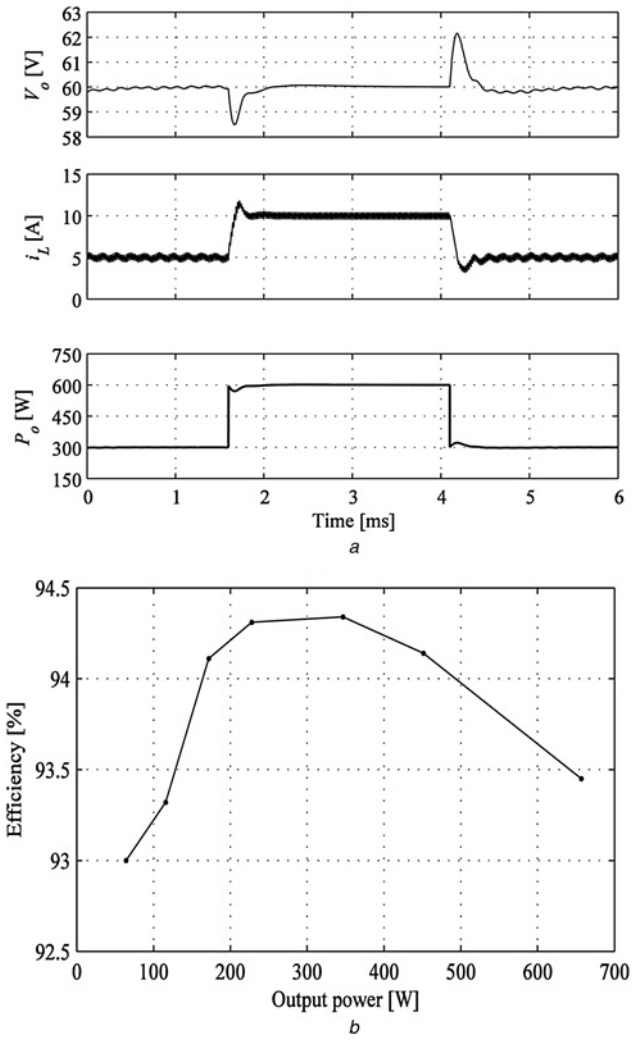

Fig. 9 *Experimental prototype tested for different loads*

a Closed-loop tests for a changing of 50% in the load
b Converter efficiency evaluation for different loads

4 Resonant reset forward converter and zeta converter similarities

In Fig. 4, the output characteristic of the resonant reset forward converter, the conventional forward and the buck–boost converter is presented to show similarities and differences between them. By analysing that figure it is possible to conclude that placing a capacitor in parallel with the rectifying diode (D_R), it changes the converter output characteristics. Therefore the resonant reset forward converter is, actually, in the first operational stage a forward converter and in the second stage an isolated zeta converter (see Fig. 2), and its output characteristics are actually more similar to an isolated zeta converter than a forward converter. Thus, to prove these similarities, it will be shown that it is possible to find the zeta converter output characteristics from the resonant reset forward converter.

In Fig. 3, the voltage across v_{CR} is working in discontinuous mode, that is, $\gamma T < DT$. Considering the converter operating in the limit between the continuous and the discontinuous mode ($\gamma T = DT$), the converter will have only two operational stages. In one stage it will operate as a zeta converter and the other in a resonant way. Thus, calculating the average voltage across the magnetising inductance, L_m, and making it equal to zero, it is possible to obtain the converter output characteristic, and is given by

$$v_{L_m} = 0$$

$$0 = \frac{1}{T}\left[\int_0^{DT}\left[v_{CR\cdot max}\left(1-\frac{t}{DT}\right)+nV_{DC}-V_o\right]dt+\int_{DT}^{T}(-V_o)dt\right] \tag{50}$$

After some mathematical manipulation it results in

$$v_{CR\cdot max} = 2\left(\frac{V_o}{D}-nV_{DC}\right) \tag{51}$$

The maximum voltage $v_{CR\cdot max}$ was already determined in (14). For small angles, according to Taylor's theorem, the tangent can be approximated by

$$\tan(x) = x+\frac{x^3}{3}+\frac{2x^5}{15}\cdots \quad \text{for } |x| < \frac{\pi}{2} \tag{52}$$

Thus, using this approximation in (14) (disregarding terms with

order superior to one), $v_{CR\cdot max}$ can be rewritten as

$$v_{CR\cdot max} = 2nV_{DC}\frac{D}{1-D} \tag{53}$$

Substituting (53) into (51), we obtain

$$\frac{V_o}{nV_{DC}} = \frac{D}{1-D} \tag{54}$$

which proves that the resonant reset forward converter has the same output characteristic as the zeta converter in the limit between the continuous and discontinuous mode. When $\gamma T < DT$ the studied converter preserves the same characteristics, as shown in Fig. 4.

5 Conclusions

In this paper the modelling, control and realisation of the single-ended forward converter with resonant reset at the secondary side is presented. This converter does not have auxiliary winding to demagnetise the transformer and presents other advantages as lower transformer size and lower peak voltage across the main switch. All these characteristics can be guaranteed placing only one capacitor in parallel with the rectifier diode at the secondary side. This additional capacitor changes the converter output characteristic, making it similar to an isolated zeta converter. Therefore it can operate as a step-up and a step-down converter.

Moreover, following the methodology described in this paper and using silicon carbide power MOSFET switches it is also possible to reach higher efficiencies (up to 94.3%) when compared with conventional forward converters.

6 Acknowledgment

The authors acknowledge the financial support provided by the Federal University of Santa Catarina.

7 References

1 Wu, H., Xing, Y.: 'Families of forward converters suitable for wide input voltage range applications', *IEEE Trans. Power Electron.*, 2014, **29**, (11), pp. 6006–6017
2 Tan, F.D.: 'The forward converter: from the classic to the contemporary'. 17th Annual IEEE Applied Power Electronics Conf. and Exposition, 2002, APEC 2002, 2002, vol. 2, pp. 857–863
3 Hong-fei, W., Xing, Y.: 'A family of forward converters with inherent demagnetizing features based on basic forward cells', *IEEE Trans. Power Electron.*, 2010, **25**, (11), pp. 2828–2834
4 Cobos, J.A., Garcia, O., Uceda, J., Sebastian, J., de la Cruz, E.: 'Comparison of high efficiency low output voltage forward topologies'. 25th Annual IEEE Power Electronics Specialists Conf., PESC '94 Record, 20–25 June 1994, vol. 2, pp. 887–894
5 Gu, Y., Gu, X., Hang, L., Du, Y., Lu, Z., Qian, Z.: 'RCD reset dual switch forward DC/DC converter'. IEEE 35th Annual Power Electronics Specialists Conf., 2004, PESC 04, 20–25 June 2004, vol. 2, pp. 1465–1469
6 Wei, Y., Wu, X., Gu, Y., Ma, H.: 'Wide range dual switch forward-flyback converter with symmetrical RCD clamp'. IEEE 36th Power Electronics Specialists Conf., 2005, PESC '05, 16–16 June 2005, pp. 420–424
7 Jovanovic, M.M., Zhang, M.T., Lee, F.C.: 'Evaluation of synchronous-rectification efficiency improvement limits in forward converters', *IEEE Trans. Ind. Electron.*, 1995, **42**, (4), pp. 387–395
8 Gu, Y., Chen, H., Lu, Z., Qian, Z., Wei, K.: 'A family of asymmetrical dual switch forward DC–DC converters'. 20th Annual IEEE Applied Power Electronics Conf. and Exposition, 2005, APEC 2005, 6–10 March 2005, vol. 3, pp. 1556–1560
9 Soltanzadeh, K., Dehghani, M., Khalilian, H.: 'Analysis, design and implementation of an improved two-switch zero-current zero-voltage pulse-width modulation forward converter', *IET Power Electron.*, 2014, **7**, (4), pp. 1016–1023
10 Chen, W., Lu, Z., Ye, S.: 'A comparative study of the control type ZVT PWM dual switch forward converters: analysis, summary and topology extensions'. 24th Annual IEEE Applied Power Electronics Conf. and Exposition, 2009, APEC 2009, 15–19 February 2009, pp. 1404–1409
11 Zhang, W., Chen, W., Yao, W., Lu, Z.: 'Analysis on rectifier diode stress issue of the DCM active clamped dual-switch forward converter and its solutions'. 24th Annual IEEE Applied Power Electronics Conf. and Exposition, 2009, APEC 2009, 15–19 February 2009, pp. 1421–1426
12 Kuo, Y.-C., Tsai, C.-T., Kuo, Y.-P., Pai, N.-S., Luo, Y.-C.: 'An active-clamp forward converter with a current-doubler circuit for photovoltaic energy conversion'. Int. Conf. on Information Science, Electronics and Electrical Engineering (ISEEE), 2014, 26–28 April 2014, vol. 1, pp. 513–517
13 Murakami, N., Yamasaki, M.: 'Analysis of a resonant reset condition for a single-ended forward converter'. 19th Annual IEEE Power Electronics Specialists Conf., 1988, PESC '88 Record, 11–14 April 1988, vol. 2, pp. 1018–1023
14 Xie, X., Zhang, J.M., Luo, G., Jiao, D., Qian, Z.: 'An improved self-driven synchronous rectification for a resonant reset forward converter'. 18th Annual IEEE Applied Power Electronics Conf. and Exposition, 2003, APEC '03, 9–13 February 2003, vol. 1, pp. 348–351
15 Chen, S.-Y., Van, M.T.: 'Accurate model for the forward converter with peak current-mode control', *IET Power Electron.*, 2013, **6**, (6), pp. 1078–1087
16 Gu, Y., Lu, Z., Qian, Z., Gu, X., Hang, L.: 'A novel ZVS resonant reset dual switch forward DC–DC converter', *IEEE Trans. Power Electron.*, 2007, **22**, (1), pp. 96–103
17 Melkonyan, A., Lorenz, L.: 'Realisation of the resonant reset ZVS forward converter for distributed power supplies using new SiC power transistor'. Conf. Record of the 2004 IEEE Industry Applications Conf., 2004. 39th IAS Annual Meeting, 3–7 October 2004, vol. 3, pp. 1805–1810
18 Spiazzi, G.: 'A high-quality rectifier based on the forward topology with secondary-side resonant reset', *IEEE Trans. Power Electron.*, 2003, **18**, (3), pp. 725–732
19 Su, B., Wen, H., Zhang, J., Lu, Z.: 'A soft-switching post-regulator for multi-outputs dual forward DC/DC converter with tight output voltage regulation', *IET Power Electron.*, 2013, **6**, (6), pp. 1069–1077
20 Yao, Z., Xiao, L.: 'Family of zero-voltage-switching unregulated isolated step-up DC–DC converters', *IET Power Electron.*, 2013, **6**, (5), pp. 862–868
21 Lin, B.-R., Huang, C.E., Wang, D.: 'Analysis and implementation of a zero-voltage switching forward converter with a synchronous rectifier', *IEE Proc., Electr. Power Appl.,* , 2005, **152**, (5), pp. 1085–1092